Length-scale dependence of pH- and temperature-response of PDMAEMA-b-PHPMA block copolymer self-assemblies in aqueous solutions

Aristeidis Papagiannopoulos[*,1], Theodoros Sentoukas[1,2], Stergios Pispas[1], Aurel Radulescu[3], Vitali Pipich[3] and Christian Lang[3]

[1]Theoretical and Physical Chemistry Institute, National Hellenic Research Foundation, 48 Vassileos Constantinou Avenue, 11635 Athens, Greece.

[2]Center of Polymeric and Carbon Materials, Polish Academy of Sciences, 34 M. Curie-Skłodowskiej, 41-819 Zabrze, Poland.

[3]Jülich Centre for Neutron Science JCNS Forschungszentrum Jülich GmbH, Outstation at Heinz Maier-Leibnitz Zentrum (MLZ), Lichtenbergstraße 1, 85747 Garching, Germany.

Email: apapagiannopoulos@eie.gr

Abstract

Amphiphilic doubly responsive block copolymers poly(2-(dimethylamino)ethyl methacrylate)-*b*-poly(hydroxy propyl methacrylate) (PDMAEMA-*b*-PHPMA) were studied by very small angle and small angle neutron scattering (VS/SANS) in aqueous solutions. A multi-level hierarchical approach was used to fit the experimental data and Bayesian analysis was performed to explore possible interdependencies between the extracted parameters. Hydrophobic contacts between the block copolymer monomers appear to create local concentration inhomogeneities (2-4 nm) whose size and mass depends on the preparation protocol. A solvent-exchange solubilization protocol leads to smaller inhomogeneities in comparison to a direct solubilization protocol due to better arrangement of the PHPMA hydrophobic units. At acidic and neutral pH hierarchical structure is observed where the local inhomogeneities are organized within aggregates (~200 nm) and grow or shrink with temperature depending on pH. At acidic pH aggregates are interconnected into large clusters.

By increasing temperature, aggregates become larger in both afcidic and neutral pH, while this response is stronger for the solvent-exchange solubilization protocol. Very interestingly, aggregates transform into self-similar superstructures at basic pH (where PDMAEMA is uncharged) to an extend that it is strongly preparation protocol-dependent. These transitions at length scales from 1 to 1000 nm open many possibilities for advanced multiple stimuli-responsive loading and release of proteins and drug molecules in such polymeric nanostructures.

1. Introduction

Amphiphilic block copolymers have been studied and utilized in a plethora of applications as drug/protein/gene delivery nanocarriers for more than three decades due to their ability to self-assemble in various formations when inserted in aqueous media. [1-3] Their final characteristics are dictated by certain physicochemical parameters, such as the solubilization protocol, block composition, molecular weight, and/or environmental factors (in the case of stimuli-responsive polymers).[4, 5] The most iconic formation is the micelle, which is comprised of a hydrophobic core and a hydrophilic corona, while aggregates of micelles are the most commonly observed.[6] The hydrophobic block can be utilized to encapsulate small drug molecules, while the hydrophilic block operates as colloidal stabilizer along with the ability to complex with biological macromolecules or inorganic particles through electrostatic interactions.[7, 8]

Stimuli-responsive polymers possess the ability to alter their chain conformation in aqueous solutions upon the change of certain environmental factors, such as temperature and pH.[5, 9-12] Poly(2-(dimethylamino)ethyl methacrylate) (PDMAEMA) is a pH and thermoresponsive polymer with a characteristic group of a tertiary amine. In pH 3 aqueous solutions the amine groups become fully protonated, increasing polymer hydrophilicity and thus presents no

thermoresponsiveness. In pH 7 and pH 10, the amine groups become semi and fully deprotonated, and PDMAEMA exhibits thermoresponsive behavior, with a transition temperature in the range of 35-55^{o}C, depending on its molecular weight and the connected block (in case of block copolymers).[13-15] Furthermore, PDMAEMA has the ability to complex with biomacromolecules through electrostatic interactions.[16-19] Poly(hydroxy propyl methacrylate) (PHPMA) is a weakly-hydrophobic polymer, with a characteristic hydroxyl group that is reported to exhibit thermoresponsiveness when block copolymerized with another hydrophilic polymer.[20-23]

Doubly thermoresponsive amphiphilic block copolymer systems can be extremely interesting, due to their ability to switch roles in the core-corona formation at certain temperatures above or below the thermoresponsive block and pH values above or below the pK_a of the pH-responsive block. Such behavior is characterized as "schizophrenic"[24, 25] and if manipulated properly can result in the desired response, size and shape of the formed nanoparticles, enabling them as potential nanocarriers for both hydrophobic and hydrophilic drugs for targeted delivery.[10, 26] Poly(2-(dimethylamino)ethyl methacrylate)-*b*-poly(hydroxy propyl methacrylate) (PDMAEMA-*b*-PHPMA) block copolymers have been reported to belong to that category, comprising of a hydrophilic pH-responsive and thermoresponsive PDMAEMA block and a weakly-hydrophobic thermoresponsive PHPMA block. Their associations' internal morphology is heavily dictated by chemical composition, solubilization protocol, temperature and pH of the aqueous solution, resulting in formations with different sizes and micro-polarities. Aqueous solution studies have indicated the possible existence of tight compound micelles or loose hydrophilic polymeric networks depending on the solubilization protocol utilized.[27] Furthermore, we have studied the complexation ability of the specific block copolymers with bovine serum albumin (BSA)[28] and salmon sperm DNA molecules [29],

and observed fragmenting of the original block copolymers aggregates into smaller biohybrid nanoassemblies via electrostatic interactions.

Small angle neutron scattering has been successfully used in the characterization of thermoresponsive synthetic and biological macromolecular associations in aqueous media with characteristic examples from poly(N-isopropylacrylamide)-containing block copolymers,[30, 31] thermoresponsive polyoxazoline copolymers,[32, 33] PDMAEMA block polyelectrolytes[34] and bionanoparticles of polysaccharides and proteins after thermal denaturation.[35] This method resolves structure at multiple length-scales from 1 to 100 nm noninvasively and averages over macroscopic volumes within the sample. In particular, structure at different length-scales has been probed in regard to the effect of added protein for thermoresponsive block copolymers [36] and in relation to loaded drugs in amphiphilic block copolymers.[37-39] The temperature response at different length scales has been also resolved in poly(n-butyl acrylate)-b-poly(N-iso-propylacrylamide)-b-poly(acrylic acid) (PnBA-b-PNIPAM-b-PAA) triblock terpolymers by our group.[40]

In the present work, a PDMAEMA-*b*-PHPMA block copolymer was utilized to study the internal chain conformation of the system via very small and small angle neutron scattering (VS/SANS). The aqueous solution preparation involved the use of a direct and a solvent-exchange solubilization protocol, since they result in different self-assembly formations of the block copolymers and the pH values of 3, 7 and 10 in a temperature range of 25-55^{o}C. VS/SANS allows the determination of hierarchical and self-similar morphology in the interior of the self-assembled PDMAEMA-*b*-PHPMA block copolymers and their response to the external stimuli of pH and temperature over a wide spatial range in the nanoscale. Bayesian inference is employed to evaluate the optimization parameters' uncertainties and

interdependencies. The findings will be very useful for studies on loading and release of proteins and molecular hydrophobic drugs.

2. Materials and Methods

2.1 Materials

PDMAEMA-*b*-PHPMA diblock copolymers were used as synthesized in previous work.[27] Acetone-D_6, DCl and NaOD, were purchased from Aldrich. D_2O (99,9%) was purchased from Eurisotop. The value of pH was set by the deuterated acid and base DCl and NaOD.

Table 1. Molecular characteristics of PDMAEMA-b-PHPMA block copolymers.

Sample	M_w (g/mol) (x 10^3)[a]	M_w/M_n[a]	DP of PDMAEMA	DP of PHPMA	%wt PDMAEMA[b]
PDMAEMA-*b*-PHPMA	16.7	1.36	32	75	30

[a] Determined by SEC

[b] Determined by ^{1}H NMR

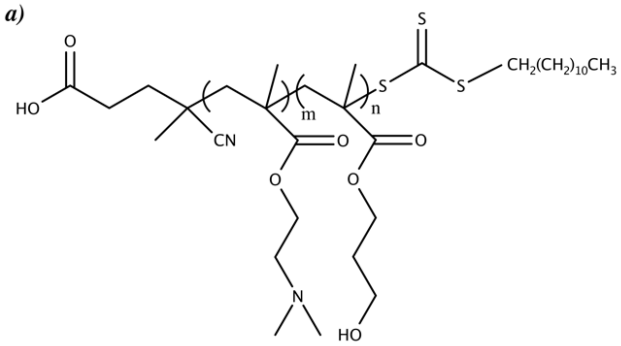

Scheme 1. Chemical structure of PDMAEMA-b-PHPMA block copolymer.

2.2 Self-assembly in D_2O

Two different solubilization protocols (denoted as A and B) were utilized for the stock solution preparation, using guidelines from previous work. Protocol A includes the preparation of the PDMAEMA-*b*-PHPMA aqueous solutions by directly dissolving the copolymers (4 mg) in deuterated water (D_2O) (1 mL). Protocol B includes the preparation of the PDMAEMA-*b*-PHPMA aqueous solutions by directly dissolving the copolymers (4 mg) into deuterated acetone (d_6) (0.1 mL) and then introducing them rapidly into deuterated water (D_2O) (1 mL) under vigorous stirring. Afterwards, the solution was left at room temperature until evaporation of the deuterated acetone. Preparation of the PDMAEMA-b-PHPMA solutions was performed at pH 7 for both protocols. In order to test pH-response, the value of pH was set by adding minute amounts of acid (DCl) or base (NaOD). For static light scattering (SLS) the same procedure was followed. The target concentration 0.2 $mgml^{-1}$ for SLS was achieved with 2 mg PDMAEMA-*b*-PHPMA for a final D_2O volume of 10 ml. The term pH will be used throughout instead of pD. Although the acidity/bacidity of the solutions are determined in 100 % D_2O there is no correction needed for the pH value for pH<8 and the error will not be greater than 0.1 at pH 10.[41]

2.3 Very small and small angle neutron scattering

Experiments were performed at the FRMII reactor (Jülich Centre for Neutron Science) on the instruments KWS-3 (VSANS diffractometer with focusing mirror) and KWS-2 (high intensity / wide-q SANS diffractometer). The neutron wavelength on KWS-3 was 12.8 Å while two sample-detector distances were chosen i.e. 1.15 and 9.15 m. For KWS-2 the wavelength was 5 Å and the sample-detector distances were 2 and 8 m. The total q-range covered was $2.01 \cdot 10^{-4}$ – $3.32 \cdot 10^{-1}$ $Å^{-1}$. A Julabo thermostat with an accuracy of 0.01 °C was used to set the sample temperature. The samples were allowed to equilibrate for longer than 30 min at the desired temperature.

Raw data was treated by standard correction and reduction procedures. 1-D scattered intensity $I(q)$ data were obtained from the collected isotropic 2-D raw data by azimuthal integration. A q-independent constant was subtracted from the experimental data representing the incoherent scattering in SANS profiles. A Gaussian function[42] was used to convolute the theoretical SANS profiles $I^{th}(q)$ in order to take instrumental resolution function $\Delta q(q)$ into account[43, 44] i.e.

$$I^{conv}(q) = \frac{1}{\sqrt{2\pi}\Delta q(q)} \int_{-\infty}^{+\infty} dq' \cdot exp\left(-\left(\frac{q'-q}{\sqrt{2}\Delta q(q)}\right)^2\right) \cdot I^{th}(q').$$

2.4 VS/SANS data optimization

Fitting procedure included the calculation of $I^{conv}(q)$ and minimization of the sum of the weighted square differences $\chi^2 = \sum_{i=1}^{N} \left(\frac{I^{conv}(P;q_i) - I^{exp}(q_i)}{\delta I^{exp}(q_i)}\right)^2$ between N theoretical and experimental intensities, where P is the set of the optimization parameters $\{P_i\}$, $I^{exp}(q_i)$ is the experimentally obtained intensity and $\delta I^{exp}(q_i)$ its uncertainty. The calculations were made with custom made code in MATLAB. Fitting algorithms were based on a Monte Carlo simulated annealing minimization scheme[45]. The Markov Chain Monte Carlo (MCMC) algorithm of Goodman and Weare[46] was implemented in order to obtain the posterior distributions of the fitted parameters. In this Bayesian analysis[47] 100 Markov chains of 1000 steps each were used after disregarding the period of the simulated annealing process to converge (burn-in period). Corner plots[48] were used in order to present any dependence between fitted parameters. Correlation coefficients between fitted parameters were calculated by $r(P_i, P_j) = \frac{1}{M-1} \sum_{k=1}^{M} \left(\frac{P_i^k - \langle P_i \rangle}{\delta P_i}\right)\left(\frac{P_j^k - \langle P_j \rangle}{\delta P_j}\right)$ where $\langle P_i \rangle$ and δP_i are the mean and standard deviation of P_i respectively over the space of the M pairs of parameters instances P_i^k and P_j^k.

2.5 Static light scattering

An ALVGmbH system with an ALV/CGS-3 compact goniometer was used for SLS. A JDS Uniphase 22 mW He-Ne laser (λ = 632.8 nm) was the light source. The average of five measurements was taken

at each angle. SLS was performed at the angular (θ) range of 30°-130°.[49] The Rayleigh ratio $R(q)$ was measured and extracted in the form $\frac{R(q)}{Kc}$. Where c is the mass concentration of the solute molecules, q is scattering wave vector $q = \frac{4\pi\, n_0}{\lambda} \sin\frac{\theta}{2}$. K stands for the LS contrast factor $K = \frac{4\pi^2 n_0^2}{N_A \lambda^4} (\frac{\partial n}{\partial c})^2$ with n_0 being the solvent's refractive index and $\frac{\partial n}{\partial c}$ the refractive index increments of the solute system. We used $\frac{\partial n}{\partial c} = 0.15\ \mathrm{mlg}^{-1}$ for all cases. A PolyScience model 9102 temperature controller/circulator was used to set the sample temperature. It was found that a 15 min wait-time was enough for the samples to equilibrate.

3. Results and Discussion

3.1 Modelling of VS/SANS data

Experiments were performed at 25, 35, 45 and 55 °C so that the room, physiological and transition temperature of the copolymers were covered. SANS experiments were used to probe inverse lengths from $2 \cdot 10^{-4}$ to $4 \cdot 10^{-1}$ Å^{-1}. This allows the determination of spatial organization of the novel block copolymers from the scale of 1 nm up to 0.5 μm. In Figures 1 and 2 the results from preparation protocol A and B respectively at 4 mgml^{-1} are shown. There are regimes of power-law behavior that span roughly one order of magnitude in q or more. These regimes are characteristic of self-similar structures and are defined by the way that macromolecules organize at the different length-scales.[50, 51]

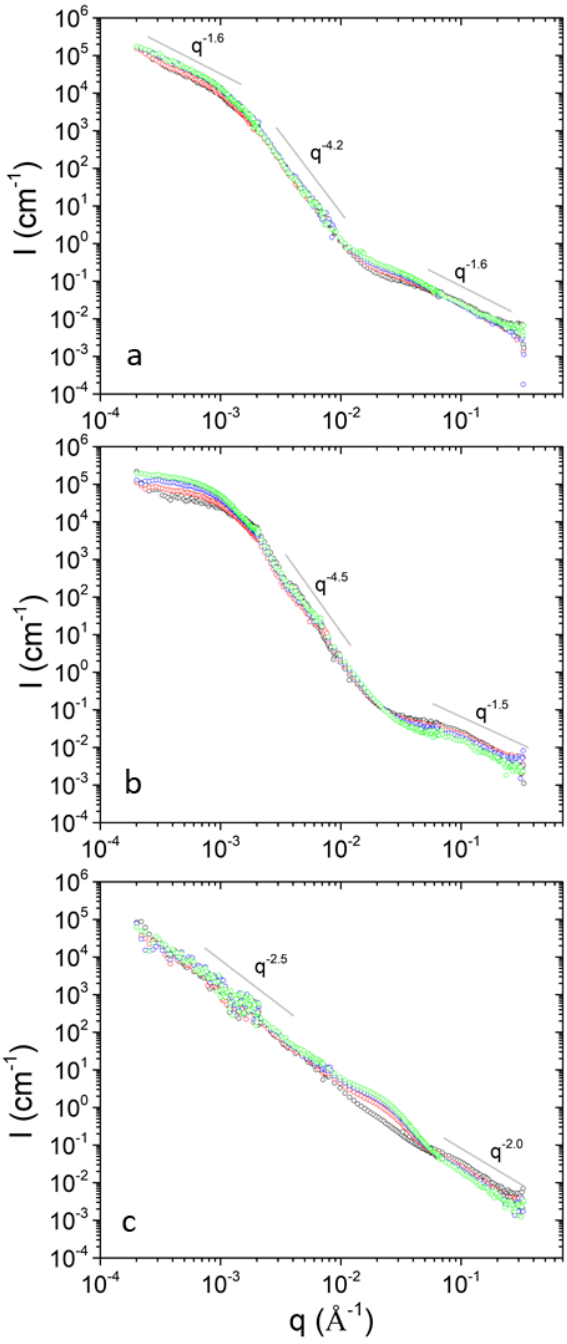

Figure 1. VS/SANS from PDMAEMA-b-PHPMA block copolymer solutions prepared by protocol A at 4 mgml^{-1} at pH 3 (a), pH 7 (b) and pH 10 (c) at 25 (black), 35 (red), 45 (blue) and 55 (green) ℃. Lines indicate power-law scaling.

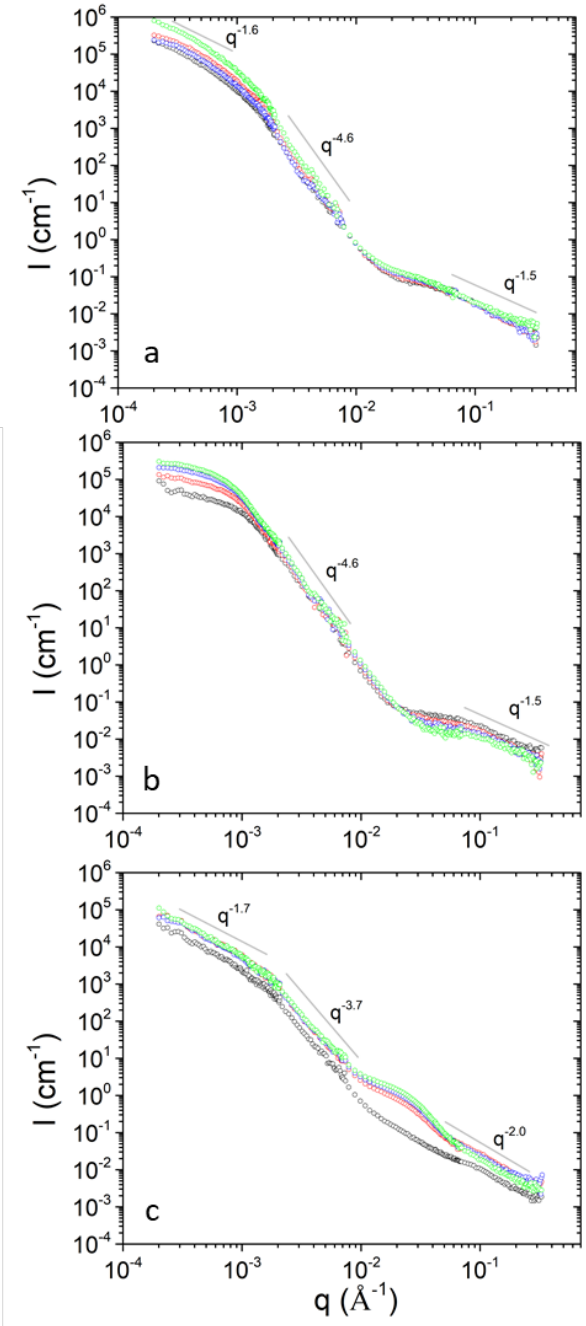

Figure 2. VS/SANS from PDMAEMA-b-PHPMA block copolymer solutions prepared by protocol B at 4 mgml^{-1} at pH 3 (a), pH 7 (b) and pH 10 (c) at 25 (black), 35 (red), 45 (blue) and 55 (green) ℃. Lines indicate power-law scaling.

SANS profiles were fitted by equation 1 which is a hierarchical Beaucage model and it is a superposition of four Beaucage terms that will be referred to as (1) clusters, (2) aggregates, (3) small-size aggregates and (4) small-size objects. The details of the separate contributions and optimization parameters are provided in the Supplementary Material. It has to be noted that in most cases less than 4 terms were used as it will be discussed in the following. The superimposed terms used for every set of data was chosen so as to provide the best fit with the least number of hierarchical levels. The terms used for every pH and temperature tested are presented in Table S1. In the multi-scale structured system, interrelated features (1-4) are characterized by their forward scattering G_i, radius of gyration $R_{g,i}$ and fractal exponent D_i which are the main extracted parameters by the fitting.

$$I(q) = \sum_{i=1}^{4} G_i \cdot exp\left(-\frac{1}{3}q^2 R_{g,i}^2\right) + B_i \cdot q^{-D_i} \cdot \left[erf\left(\frac{q \cdot R_{g,i}}{\sqrt{6}}\right)\right]^{3D_i} \cdot exp\left(-\frac{1}{3}q^2 R_{cut,i}^2\right) \quad (1)$$

3.2 Bayesian analysis on posterior distribution of VS/SANS fitted parameters

The mutual dependencies between the fitted parameters P_i and their uncertainties can be extracted by performing an analysis on the Markov Chain Monte Carlo random walks in the parameter space to investigate the reliability of the applied VS/SANS model. The analysis is performed on random walks after the convergence of the simulated annealing algorithm. Representative sets of fitted data are selected from the three different pH values to visualize the parameter interdependencies and distributions. Namely, pH 3 25 °C protocol A, pH 7 35 °C protocol B and pH 10 45 °C protocol A (at 4 mgml^{-1}) for models using hierarchical level 1, 2 and 4 (group i), 2 and 4 (group ii) and 1, 3 and 4 (group iii) respectively. The corner plots of Figure 3 present the distributions of the relative deviations of fitted parameters P_i from their optimum values P_i^{opt} i.e. $\frac{P_i - P_i^{opt}}{P_i^{opt}}$. The distributions of the individual parameters, from which the standard deviation can be extracted, are also shown (diagonal elements of corner plots). The probability distributions have been normalized to unity in regard to their maximum value

(color bar of Figure 3). The correlation coefficients r of every pair of parameters have been calculated and the interdependency has been categorized as "negligible" for $0 \leq |r| < 0.1$," weak" for $0.1 \leq |r| < 0.4$, "moderate" for $0.4 \leq |r| < 0.7$, "strong" for $0.7 \leq |r| < 0.9$ and "very strong" for $0.9 \leq |r|$. The values of r are shown in the Supplementary Material (Table S2) and are representative for the parameters from fits with models belonging to the same group. Similarly, the uncertainties presented in Table S3 represent the fitted parameters from fits belonging in the same group.

In most cases correlations between parameters are negligible, in some of them they are moderate and in very few occasions they are strong or very strong. It has to be noted that strong or very strong correlations appear between parameters that belong to the same hierarchical level and do not occur between parameters of different levels (Figure 3). This means that the parameters of the separate scattering functions are independent from each other which justifies the use of the separate hierarchical levels. Very strong correlations appear in pairs of forward scattering and radius of gyration. This is between G_2 and $R_{g,2}$ and G_4 and $R_{g,4}$ in pH 3 at 25 °C under protocol A (Figure 3a) and between G_4 and $R_{g,4}$ in pH 10 at 45 °C under protocol A (Figure 3c). This positive correlation between G and R_g (Table S2) in Guinier regimes shows that there is a region of values in the 2D space where increasing both of the parameters may lead to equally good fit. However, the uncertainty in the determination of the two values is still small i.e. between 4 and 6% for G and between 2 and 5% for R_g (Table S3). Similarly, strong correlation is found for the pairs G_2-$R_{g,2}$ and G_4-$R_{g,4}$ in pH 7 35 °C under protocol B (Figure 3b) and G_3-$R_{g,3}$ in pH 10 45 °C under protocol A (Figure 3c).

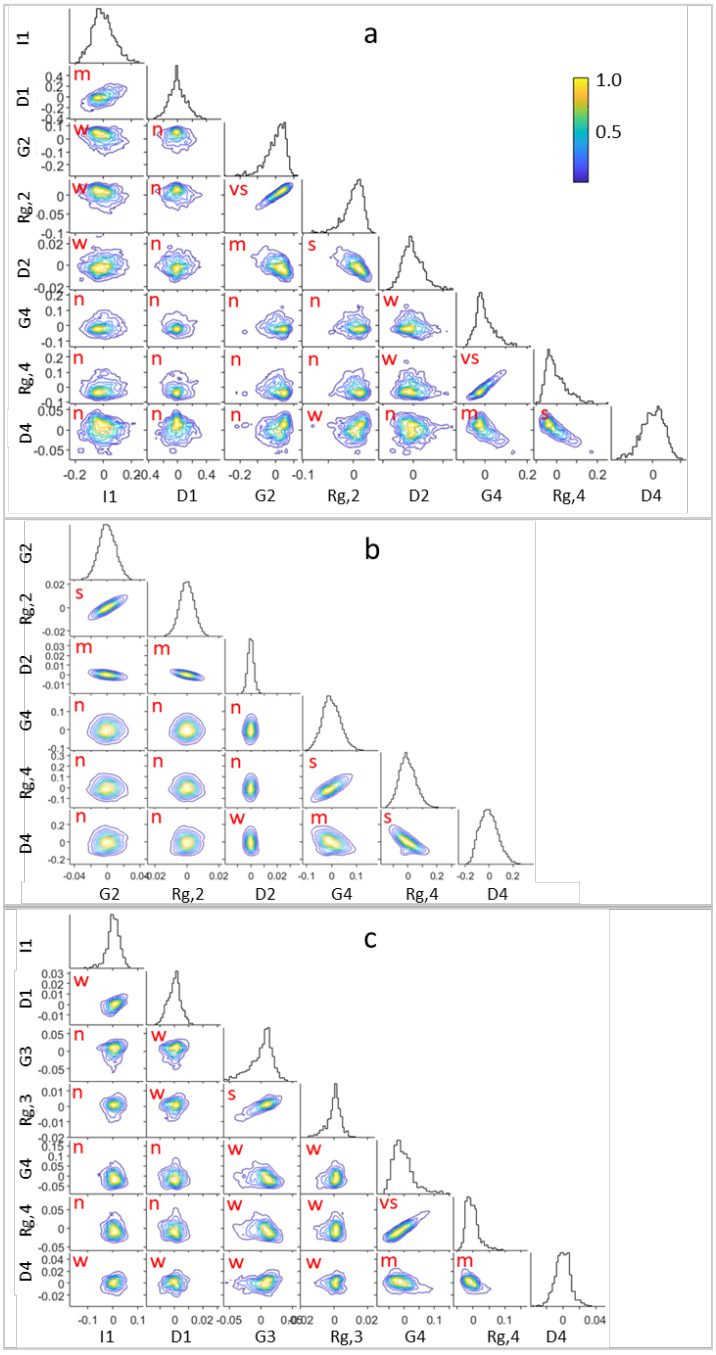

Figure 3: Corner plots of fitted parameters from PDMAEMA-b-PHPMA at 4 mgml^{-1} with (a) protocol A at pH 3 and 25 °C, (b) protocol B at pH 7 and 35 °C and (c) protocol A at pH 10 and 45 °C. Interdependencies are shown as “n” for negligible, “w” for weak, “m” for moderate, “s” for strong and “vs” for very strong.

Strong negative correlation is found between radii of gyration and fractal exponents within the same hierarchical levels. These appear in $R_{g,2}$-D_2 and $R_{g,4}$-D_4 in pH 3 25 °C under protocol A (Figure 3a) and $R_{g,4}$-d_4 in pH 7 35 °C under protocol B (Figure 3b). Therefore, there is a region where the parameters within the pairs can change in the opposite direction without affecting the fitting result. The uncertainty is still small i.e. between 1 and 2% for G, between 0.5 and 6% for R_g and between 2 and 8% for D (Table S3). Consequently, the Bayesian analysis provides the limits of uncertainty for the estimated parameters and justifies the discussion on the extracted results.

3.3 Morphology of the PDMAEMA-b-PHPMA self-assembled nanostructures and response to the external stimuli of temperature and pH

Intra- and inter-chain hydrophobic contacts are expected to form between PHPMA-PHPMA, PDMAEMA-PHPMA and PDMAEMA-PDMAEMA groups. PHPMA has hydrophobic properties which increase with its molar mass even at room temperature.[52] PDMAEMA is an intrinsically hydrophobic polyelectrolyte.

The hydrophobic domains will possibly have the ability to attract hydrophobic substances e.g. low molecular weight hydrophobic drugs. Indeed I_1/I_3 ratio for the PDMAEMA-*b*-PHPMA from Protocol B was 1.15, depicting the existence of hydrophobic domains. On the other hand, the same copolymers from Protocol A presented a I_1/I_3 ratio of 1.8, revealing the existence of hydrophilic networks within the structure.[27] It has to be reminded that the I_1/I_3 ratio, where I_1 and I_3 are the intensities of the first (372 nm) and third (383 nm) vibronic peaks in the pyrene spectrum, is customarily used to characterize the polarity of the microenvironment that surrounds the chromophore.[53-55] A value near 1.0 reveals a nonpolar environment whereas a value near 1.9 corresponds to a highly polar environment. Globular proteins contain

hydrophobic and pH dependent surface charge distributions and may interact with the interior of the aggregates by electrostatic and hydrophobic interactions. Therefore, the presented nanostructures are candidates for applications in doubly responsive loading and release of nm-sized bioactive substances.[28, 29]

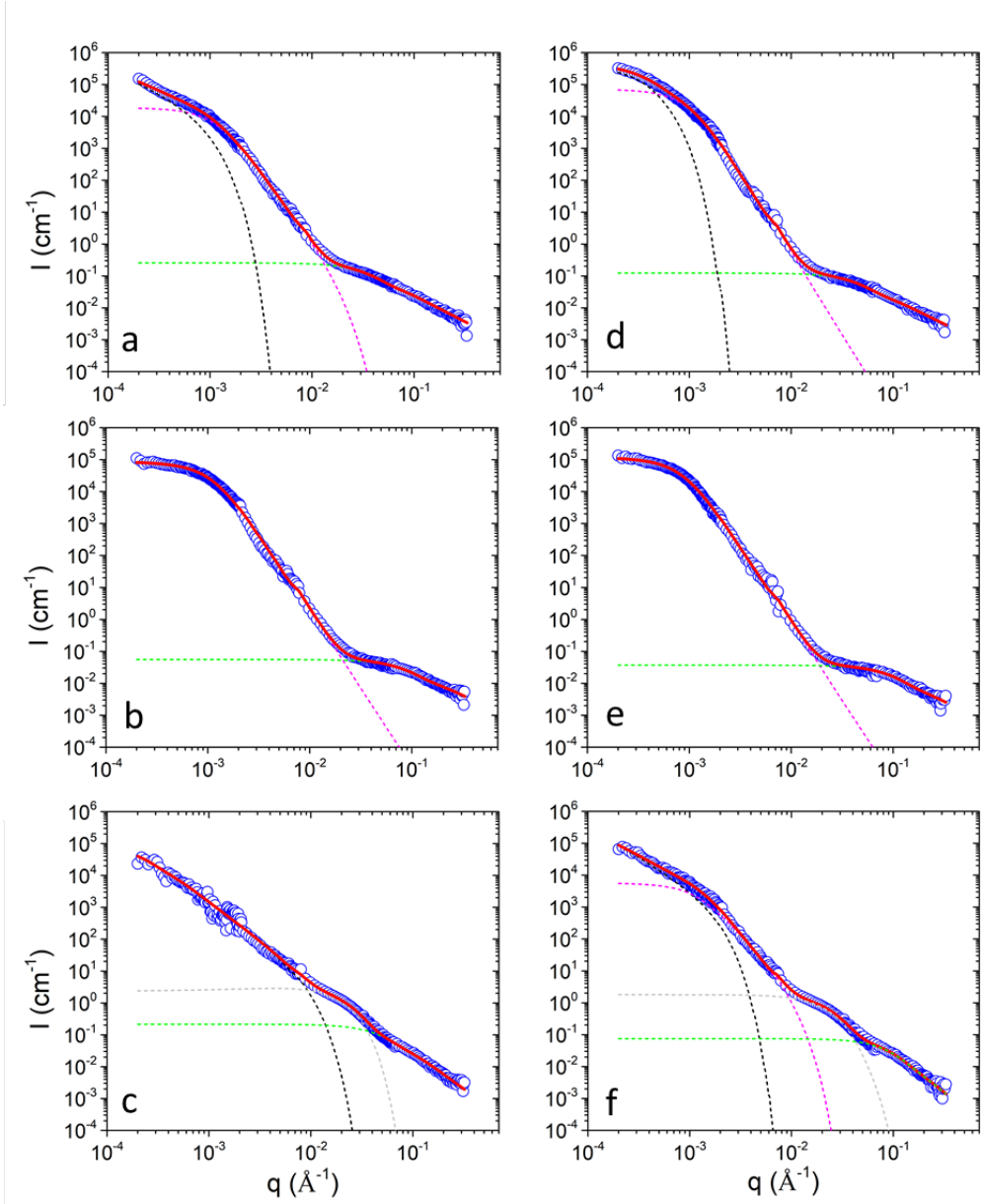

Figure 4. VS/SANS from PDMAEMA-b-PHPMA block copolymer solutions prepared by protocol A (a-c) and protocol B (d-f) at 4 mgml^{-1} at pH 3 (a,d), pH 7 (b,e) and pH 10 (c,f) at 35 °C. Red lines are best fits with equation 1. Dashed lines represent contribution from clusters (black), aggregates (magenta), small-size aggregates (gray) and small-size objects (green).

At pH 3 hierarchical self-assembly is evident (Figures 1a and 2a) for both protocols. At this pH PDMAEMA is fully protonated and not thermoresponsive.[14, 56] PHPMA presents thermoresponsiveness when copolymerized with another hydrophilic block, however without an LCST behavior but rather with an order-to-order transition. Hydroxyl groups tend to form weak hydrogen bonds with hydrophilic side-groups, in this case ester or amino groups of PDMAEMA, while temperature rise leads to breakage of these bonds, resulting in gradual aggregation.[21, 27, 57, 58]

In protocol B PHPMA is initially in good solvent conditions (acetone). Upon mixing with water at pH 7 it experiences a mixed solvent which gradually becomes bad as acetone gradually evaporates. Therefore, hydrophobic contacts will have the ability to self-organize into a state that is closer to thermodynamic equilibrium favoring the formation of well-defined hydrophobic domains. This state would resemble a tight compound micelle configuration with a more hydrophobic nature. The inner cores, would contain mostly of PHPMA blocks, with their hydroxyl groups forming weak hydrogen bonds with each other.[27] In protocol A, where the block copolymer is directly dispersed in water, random inter-chain connections will form immediately with very small ability to be destroyed and recombined towards an equilibrium state. This configuration is expected to be similar to a loose hydrophilic network, in which hydroxyl groups of PHPMA form weak hydrogen bonds with the amino groups of PDMAEMA.[27]

The VS/SANS data were fitted with a three-level hierarchical model (Figure 4a and d) that includes clusters, aggregates and small-size objects (i.e. levels 1, 2 and 4). The uncertainty in the measured scattered intensity $\delta I^{exp}(q_i)$ is in general smaller than the size of the data points. Error bars are omitted in the plots for the sake of clarity; however, an example is provided in Figure S1. A weak upturn at low q with apparent scaling $I(q) \sim q^{-1.6}$ indicates the formation

of clusters with open mass fractal structure.[59] The parameters G_1 and $R_{g,1}$ (not shown) cannot be independently estimated because the Guinier regime of this level is outside the measurement window i.e. $R_{g,1}^{-1}<<q_{min}$ with $q_{min} \approx 2 \cdot 10^{-4}$ Å^{-1}. Nevertheless, the contribution of this hierarchical level at the lowest q ($I_1^{q_{min}}$) is presented for comparisons (Table 2). This scattering contribution is enhanced at higher temperatures i.e. 45 and 55 °C for protocol A and 55 °C for protocol B. Protocol B has a stronger scattering contribution of clusters at all temperatures and a stronger relative temperature response in comparison to protocol A. The characteristic fractal exponents are the ones expected from clusters with open structure although the q-range within which the scattering contribution of clusters dominates is quite limited (Figure 4a and d and Table 2). The presence of more compact hydrophobic domains in protocol B enhances clustering possibly by bridging interactions between aggregates. Additionally, the thermal response of clustering represented by $I_1^{q_{min}}$ is more effective in this state.

Table 2. VS/SANS-extracted parameters from PDMAEMA-b-PHPMA block copolymer solutions at pH 3 with concentration 4 mgml^{-1}.

Protocol	A				B			
Parameter\Temp.	25 °C	35 °C	45 °C	55 °C	25 °C	35 °C	45 °C	55 °C
$I_1^{q_{min}}$ $(10^3 cm^{-1})$	109	103	151	150	188	239	189	544
D_1	2.17	1.94	1.91	2.40	1.65	1.70	1.67	1.36
G_2 $(10^3 cm^{-1})$	26.9	18.9	21.6	58.3	37.3	72.2	68.4	150
$R_{g,2}$ (nm)	185	172	180	225	207	212	228	215
D_2	4.48	4.37	4.32	4.01	4.67	5.08	4.80	5.50
G_4 (cm^{-1})	0.149	0.256	0.319	0.350	0.0898	0.123	0.141	0.180
$R_{g,4}$ (nm)	3.57	4.94	5.15	6.57	3.03	3.79	3.95	4.50
D_4	1.58	1.63	1.54	1.48	1.57	1.57	1.65	1.43

At intermediate q the apparent behavior $I(q)\sim q^{-4.2}$ shows that aggregates with well-defined interfaces are formed in protocol A (Figure 1a). Porod's law predicts $I(q)\sim q^{-4}$ at $q>>R_g^{-1}$ (where R_g is the radius of gyration) for objects with perfectly smooth interface. However, power-laws $I(q)\sim q^{-n}$ with exponents n higher than 4 are expected for objects with diffuse interface.[60, 61] The situation is similar at intermediate q for protocol B (Figure 2a) with apparent scaling $I(q)\sim q^{-4.6}$. The numerically extracted characteristic exponents are between 4 and 5 and are somewhat higher for protocol B (Table 2). Protocol A produces somewhat smaller aggregates than protocol B ($R_{g,2}$) and of lower mass which is related to G_2.[62] This is possibly because of the formation of more compact hydrophobic domains that apparently favor stronger aggregation in B. The values of $R_{g,2}$ are in the order of 200 nm and increase with temperature. The increase in the forward scattering G_2 with temperature is strong for both protocols. Temperature response is stronger for protocol B in regard to G_2 (27 to $58\cdot10^3$ cm^{-1} in A and 37 to $150\cdot10^3$ cm^{-1} in B) and weaker in regard to $R_{g,2}$ (185 to 225 nm in A and 207 to 215 nm in B). This indicates that upon temperature increase the reorganization has a different mechanism to enhance aggregation. In the presence of more compact hydrophobic domains that contain PHPMA (protocol B) densification of aggregates occurs whereas in more randomly connected networks (protocol A) aggregates grow in size.

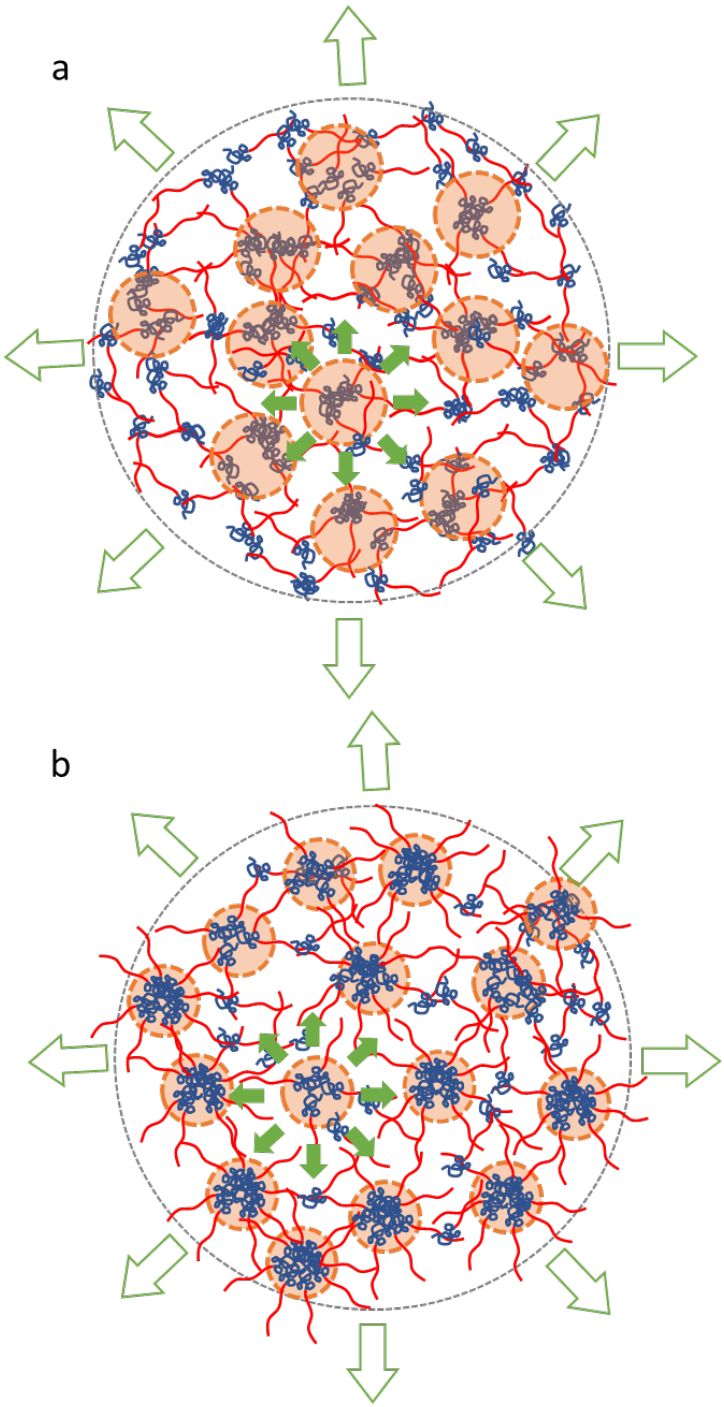

Scheme 2. Illustration of PDMAEMA-b-PHPMA block copolymer aggregates and their internal structure in protocol A (a) and B (b) at pH 3. PDMAEMA (red) and PHPMA (blue) blocks are shown. Large and small circles indicate aggregates and small objects respectively. Open and closed arrows indicate temperature response of aggregates and small objects respectively.

At high q (higher than $2 \cdot 10^{-2}$ Å^{-1}) the scattering from small objects dominates (Figures 1a and 2a). These objects can be considered on the basis of characteristic inhomogeneities in cross-linked networks.[63-66] In that case cross-linking creates local density fluctuations that are frozen in space and are not able to relax by diffusion. In the case of PHPMA-b-PDMAEMA one can think of the inhomogeneities originating from hydrophobic contacts. Forward scattering G_4 and size $R_{g,4}$ are larger in protocol A in comparison to protocol B. In protocol A the inhomogeneities are regions of higher concentration within the formed network that contain chain segments from both copolymers. In protocol B they consist mostly of PHPMA compact domains. In protocol A these inhomogeneities ($R_{g,4} \approx 3.6$ nm) are larger than in protocol B ($R_{g,4} \approx 3.0$ nm). The characteristic exponent is about 1.5-1.6 (good solvent conditions) for both protocols and it could be related to the configuration of individual macromolecular chain segments that are free of intermolecular contacts i.e., in the space between the inhomogeneities (Table 2). Upon temperature increase small-size objects of protocol A show somewhat stronger increase in G_4 and $R_{g,4}$ than the ones of protocol B. In protocol A the segments of PHPMA are less localized in the 3D space and therefore new PHPMA units can be incorporated from the outer regions to the existing inhomogeneities than in the case of compact hydrophobic domains of protocol B. An illustration of the morphology of the PHPMA-b-PDMAEMA aggregates at room temperature is provided in Scheme 2. In protocol A the small objects consist of larger domains with mixed hydrophobic and hydrophilic segments while in protocol B small objects consist of smaller domains of mostly hydrophobic PHPMA segments. The enhancement in size and scattering strength for both hierarchical levels as temperature increases is also indicated.

At pH 7 there is no significant contribution from large clusters as a Guinier plateau is found at low q for all temperatures and for both protocols (Figures 1b and 2b). There is a weak deviation

from the Guinier behavior at low q in the case of protocol B (Figure 2b and 4e) which implies some cluster contribution. However, the aggregates' scattering dominates. The data at this pH are fitted with a combination of aggregates and small-size objects (i.e. levels 2 and 4) (Figure 4b and e). This Guinier regime represents scattering from the aggregates at $q<<R_g^{-1}$ which is followed by a power-law $I(q)\sim q^{-4.5}$. Objects with rough interfaces are observed as in the case of pH 3. Their size is in the order of 100-200 nm and 200-300 nm for protocol A and B respectively (Table 3).

The formation of clusters by decreasing pH from 7 to 3 is related to the pH-sensitive block PDMAEMA which is moderately charged at pH 7 and highly charged at pH 3. Apparently, extension of PDMAEMA conformation (pH 3) encourages bridging interactions between aggregates at room temperature. The forward scattering from aggregates G_2 increases from about 27 to $48 \cdot 10^3$ cm^{-1} and from 37 to $50 \cdot 10^3$ cm^{-1} for protocols A and B respectively between pH 3 and pH 7 (Tables 2 and 3). Regarding size, $R_{g,2}$ decreases from about 185 to 139 nm in protocol A whereas in B slightly increases from 207 to 215 nm. Therefore, aggregates lose mass and become less dense when pH drops due to the local expansion of PDMAEMA chains. At the same time this extension leads to inter-aggregate associations. Alternatively, this effect can be viewed as an incomplete dissociation of aggregates that after swelling towards disintegration remain connected in the form of clusters.

Table 3. VS/SANS-extracted parameters from PDMAEMA-b-PHPMA block copolymer solutions at pH 7 with concentration 4 mgml^{-1}.

Protocol	A				B			
Parameter\Temp.	25 °C	35 °C	45 °C	55 °C	25 °C	35 °C	45 °C	55 °C
G_2 $(10^3 cm^{-1})$	47.6	84.1	132	187	50.1	117	220	298

$R_{g,2}\ (nm)$	139	186	194	205	215	239	258	273
D_2	5.40	4.77	4.88	4.88	4.73	4.79	4.85	4.75
$G_4\ (cm^{-1})$	0.0845	0.0553	0.0369	0.0331	0.0494	0.0367	0.0318	0.0210
$R_{g,4}\ (nm)$	2.63	1.97	2.02	2.25	1.84	1.75	2.19	1.61
D_4	1.48	1.52	1.43	1.50	1.52	1.71	1.49	1.54

A strong increase of the Guinier plateau is observed as temperature increases i.e. from 48 to $187 \cdot 10^3$ cm^{-1} and from 50 to $298 \cdot 10^3$ cm^{-1} for protocols A and B respectively (Table 3) which directly signifies the enhancement of the aggregates' mass. At pH 7, PDMAEMA is partially protonated, resulting in weaker hydrogen bonds of its amino groups with water molecules and thus presents an LCST in the range of 35°C – 55°C, depending on its DP and the copolymerized block.[14, 56] PHPMA still presents a thermosensitive character as described above, gradually contributing to intermolecular associations.[21, 27, 57, 58] Therefore, the strong enhancement of aggregation is driven by both blocks and it is stronger than the one at pH 3 (Tables 2 and 3), nevertheless no precipitation occurred even past the LCST of PDMAEMA. Radii of gyration $R_{g,2}$ also increase with temperature from 139 to 205 nm for protocol A and from 215 to 273 nm for protocol B. The stronger temperature response of the aggregates' mass of protocol B (from 50 to $298 \cdot 10^3$ cm^{-1}) in comparison to protocol A (from 48 to $187 \cdot 10^3$ cm^{-1}) can be connected to the fact that in B compact hydrophobic domains are present in contrast to the more diffuse domains in A as discussed above regarding pH 3.

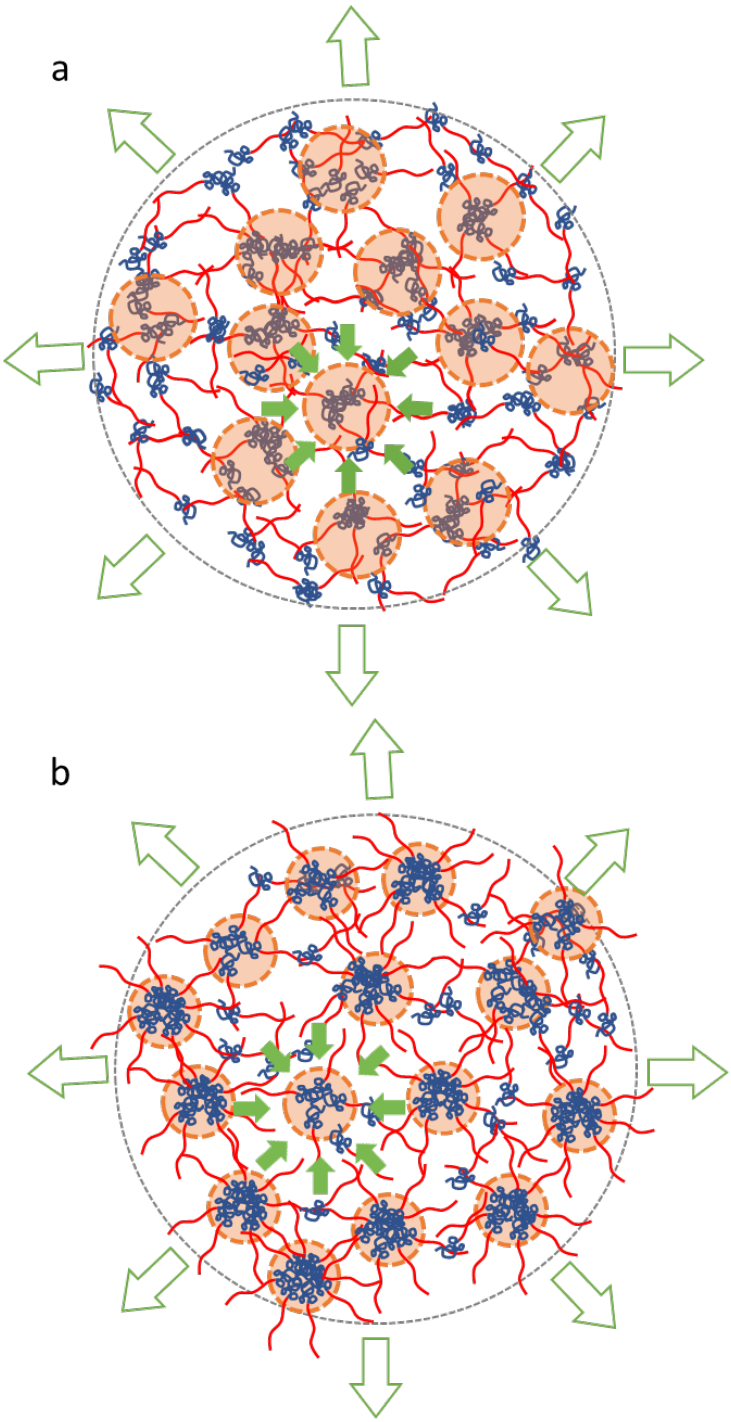

Scheme 3. Illustration of PDMAEMA-b-PHPMA block copolymer aggregates and their internal structure in protocol A (a) and B (b) at pH 7. PDMAEMA (red) and PHPMA (blue) blocks are shown. Large and small circles indicate aggregates and small objects respectively. Open and closed arrows indicate temperature response of aggregates and small objects respectively.

The radius of gyration $R_{g,4}$ is about 2-2.5 nm for the two protocols which is smaller than the one at pH 3 (higher than 3 nm) at room temperature. Additionally, forward scattering G_4 is lower at pH 7 (0.085 cm^{-1} in A and 0.049 cm^{-1} in B) in comparison to pH 3 (0.15 cm^{-1} in A and 0.090 cm^{-1} in B) (Tables 2 and 3). Mass and size of small-size objects is smaller showing that interconnections are less favorable also at this length scale. This is an effect of the less extended conformation of PDMAEMA at pH 7. Interestingly, scattering at q higher than $4 \cdot 10^{-2}$ $Å^{-1}$ systematically decreases as temperature increases (Figures 1b and 2b) and so does G_4 (Table 3). Possibly, segments of chains with no hydrophobic contacts consist mostly of PDMAEMA units. Upon temperature increase these segments contract and apply a stress on the inhomogeneities (discussed previously) that contain hydrophobic domains and act as effective crosslinks. Although hydrophilic-to-hydrophobic thermal transition occurs also inside the small-size objects (because of both PDMAEMA and PHPMA thermal transition) the net effect is a decrease of mass and size of the hydrophobic domains. The characteristic exponent D_4 is about 1.5-1.6 (good solvent conditions) for both protocols and is related to individual macromolecular chain segments that are free of hydrophobic contacts as at pH 3 (Table 3). An illustration of the morphology of the PHPMA-b-PDMAEMA aggregates at pH 7 is provided in Scheme 3. It qualitatively resembles the one of pH 3 (Scheme 2) with the difference that the scattering contribution of small objects decreases as a function of temperature.

By increasing pH from 7 to 10 the qualitative differences between the two protocols become even more evident. In protocol A (fitted with levels 1, 3 and 4) low and intermediate q scattering is dominated by a single power-law $I(q) \sim q^{-2.5}$ which covers two orders of magnitude in q (Figure 1c) and it is temperature independent (Table 4). The fitted value for the single power-law is $D_1 \approx 2.4 - 2.6$. Apparently, large self-similar structures are formed (with

$R_g^{-1} << q_{min}$). Their internal correlations reveal moderately dense mass fractals.[59] In protocol B (fitted with levels 1, 2, 3 and 4) hierarchically organized morphology is found at this q range (Figure 2c, Figure 4f and Table 4). Scattered intensity $I_1^{q_{min}}$ increases strongly from 25 °C to higher temperatures. The characteristic scaling exponent at low q is $D_1 \approx 1.6 - 1.8$ (open mass fractals) and at intermediate q is $D_2 \approx 3.4 - 3.7$ (fractally rough interfaces).[67] The radius of gyration $R_{g,2}$ of these aggregates is 190 nm which is smaller than the size of aggregates at pH 7. Forward scattering G_2 is almost an order of magnitude lower than the one at neutral pH. $R_{g,2}$ and G_2 decrease as a function of temperature. At pH 10, PDMAEMA is uncharged and thermoresponsive. It seems that contraction of the chains that form the interconnected network within the aggregates leads to breakage of hydrophobic contacts and formation of smaller aggregates.

VS/SANS intensity is found to increase as a function of temperature at q from $1 \cdot 10^{-2}$ Å^{-1} to $7 \cdot 10^{-2}$ Å^{-1} revealing the appearance of small-size aggregates (Figures 1c, 2c, 3c, 3f and Table 4). These aggregates (level 3) result from the stabilization of structures of lower size in comparison to the aggregates at pH 3 and 7. Their scattering dominates a limited q range and therefore only its Guinier regime characteristics G_3 and $R_{g,3}$ are extracted. Their forward scattering G_3 increases with temperature while their size $R_{g,3}$ is about 8 nm for all temperatures where these aggregates exist i.e. 35, 45 and 55 °C, possibly showing that their number increases. The opposite temperature response is found at q higher than $7 \cdot 10^{-2}$ Å^{-1}. Small-size objects' forward scattering G_4 and size $R_{g,4}$ appears fairly unchanged between 35 and 55 °C. The characteristic exponent D_4 is about 2-2.5 for both protocols (Table 4). This signifies a more compact average conformation of chains that are outside the inhomogeneities (in contrast to pH 3 and pH 7) as PDMAEMA is uncharged.

Table 4. VS/SANS-extracted parameters from PDMAEMA-b-PHPMA block copolymer solutions at pH 10 with concentration 4 mgml^{-1}.

Protocol	A				B			
Parameter\Temp.	25 °C	35 °C	45 °C	55 °C	25 °C	35 °C	45 °C	55 °C
$I_1^{q_{min}}$ $(10^3 cm^{-1})$	50.1	39.9	48.6	60.8	33.8	82.1	80.2	89.4
D_1	2.63	2.39	2.47	2.57	1.62	1.77	1.77	1.74
G_2 $(10^3 cm^{-1})$	-	-	-	-	7.50	5.33	5.16	4.93
$R_{g,2}$ (nm)	-	-	-	-	190	149	148	156
D_2	-	-	-	-	3.73	3.38	3.39	3.30
G_3 (cm^{-1})	-	0.871	1.68	2.50	-	1.79	2.63	2.98
$R_{g,3}$ (nm)	-	7.89	7.76	7.80	-	8.58	8.52	8.04
D_3	-	-	-	-	-	2.78	2.79	2.78
G_4 (cm^{-1})	0.0587	0.214	0.218	0.223	0.0724	0.0750	0.0833	0.0722
$R_{g,4}$ (nm)	2.52	3.50	3.47	3.42	3.49	1.94	2.25	2.21
D_4	2.20	2.22	2.17	2.29	1.92	2.55	2.29	2.47

At basic pH, PDMAEMA is fully deprotonated and weakly hydrophilic, leading to a more intense LCST transition, in which it practically becomes hydrophobic.[14, 56] The small-size objects can be again attributed to hydrophobic domains related to interconnections between segments from both blocks (by PHPMA-PHPMA, PDMAEMA-PHPMA and PDMAEMA-PDMAEMA). At pH 7 these domains are incorporated in well-defined aggregates with diffuse interface. At pH 10, these aggregates transform into large mass fractals in protocol A. This remarkable transformation implies that small-size objects arrange in a long-range self-similar structure. No precipitation is observed, even past the LCST point of PDMAEMA, in contrast with other studies in this pH,[68] depicting the fact that PHPMA's hydroxyl groups might play an important role in stabilizing the nanostructures by possible interacting with the OH ions in the solution. To some extent, the isotopic effect could also be responsible for this effect. Shifts

of cloud points to higher temperatures have been reported for thermoresponsive polymers in D_2O in comparison to H_2O as a hydrogen bond in heavy water is stronger.[69, 70]

The change of PHPMA from hydrophobic to water-soluble causes a reduction to the contacts within the preformed inhomogeneities significantly "diluting" the morphology that was created at pH 7. This transition seems incomplete in protocol B. Cluster formation reveals interconnection of aggregates and could signify the onset of the transition towards a large fractal. However, the compact domains of protocol B seem to resist complete transformation to a large fractal object. The internal structure of the aggregates has a characteristic exponent of rough interfaces i.e. $3 < d_2 < 4$ revealing compact structures. This also implies the incomplete transition towards a mass fractal in protocol B. An illustration of the morphology of the PHPMA-b-PDMAEMA morphology at pH 10 at room temperature is provided in Scheme 3. In protocol A the boundaries of aggregates are not shown because the self-similar structure spans the whole VS/SANS-accessible space. In protocol A small objects consist of domains with mixed PHPMA and PDMAEMA segments while in protocol B small objects consist of domains of mostly PHPMA segments that have been well-formed at pH 7 and did not completely disintegrate.

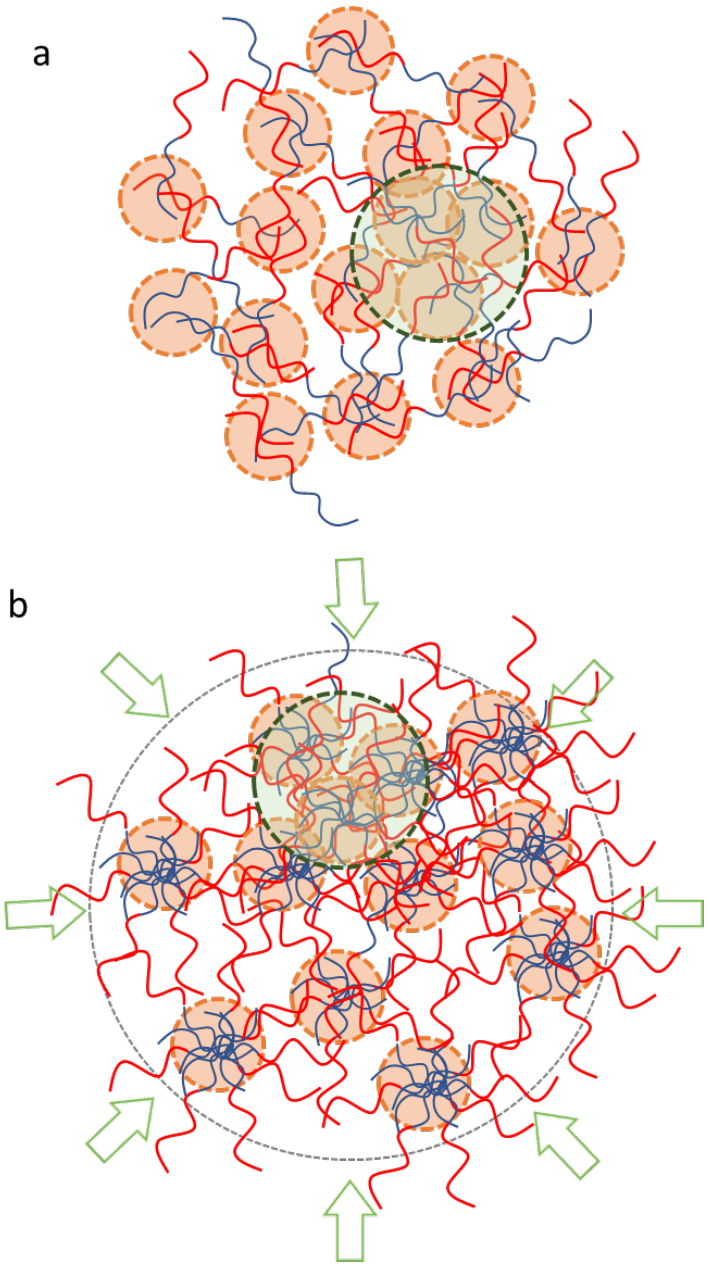

Scheme 4. Illustration of PDMAEMA-b-PHPMA block copolymer clusters internal structure in protocol A (a) and aggregates and their internal structure in protocol B (b) at pH 10. PDMAEMA (red) and PHPMA (blue) blocks are shown. Large, intermediate (that appear above 25 °C) and small circles indicate aggregates, small-size aggregates and small objects respectively. Arrows indicate temperature response of aggregates.

Thermal response of PDMAEMA (occurring at pH 10) gives rise to the creation of small-size aggregates. In protocol A these aggregates are arranged in a large fractal network. The more random distribution of PDMAEMA units within the network in contrast to PHPMA units allows the formation of small-aggregates (larger than the size of inhomogeneities) at elevated temperatures when PDMAEMA is strongly thermoresponsive (pH 10).

These findings would have very strong impact on the loading and release of hydrophobic and charged substances by the self-assembled PHPMA-b-PDMAEMA nanostructures. At pH 3 and 7 thermal response enhances the formation of aggregates in both protocols, however it enhances small objects at pH 3 and weakens them at pH 7. Additionally, diffuse or more localized and compact hydrophobic domains are formed in protocol A or B respectively. At pH 10 a tremendous change occurs towards the formation of large self-similar loose fractals with a difference in the extent of this transformation between the two protocols. Thermal response is accompanied with formation of small-size aggregates. These morphology transitions would affect both the transport and interactions of encapsulated drugs and proteins. General examples would include administration of loaded carriers from storage (temperature lower than or equal to 25 °C) to the human body (temperature higher than 35 °C) and transport of anticancer drugs-loaded aggregates to the small intestine (acidic environment) via the stomach (basic environment).[71]

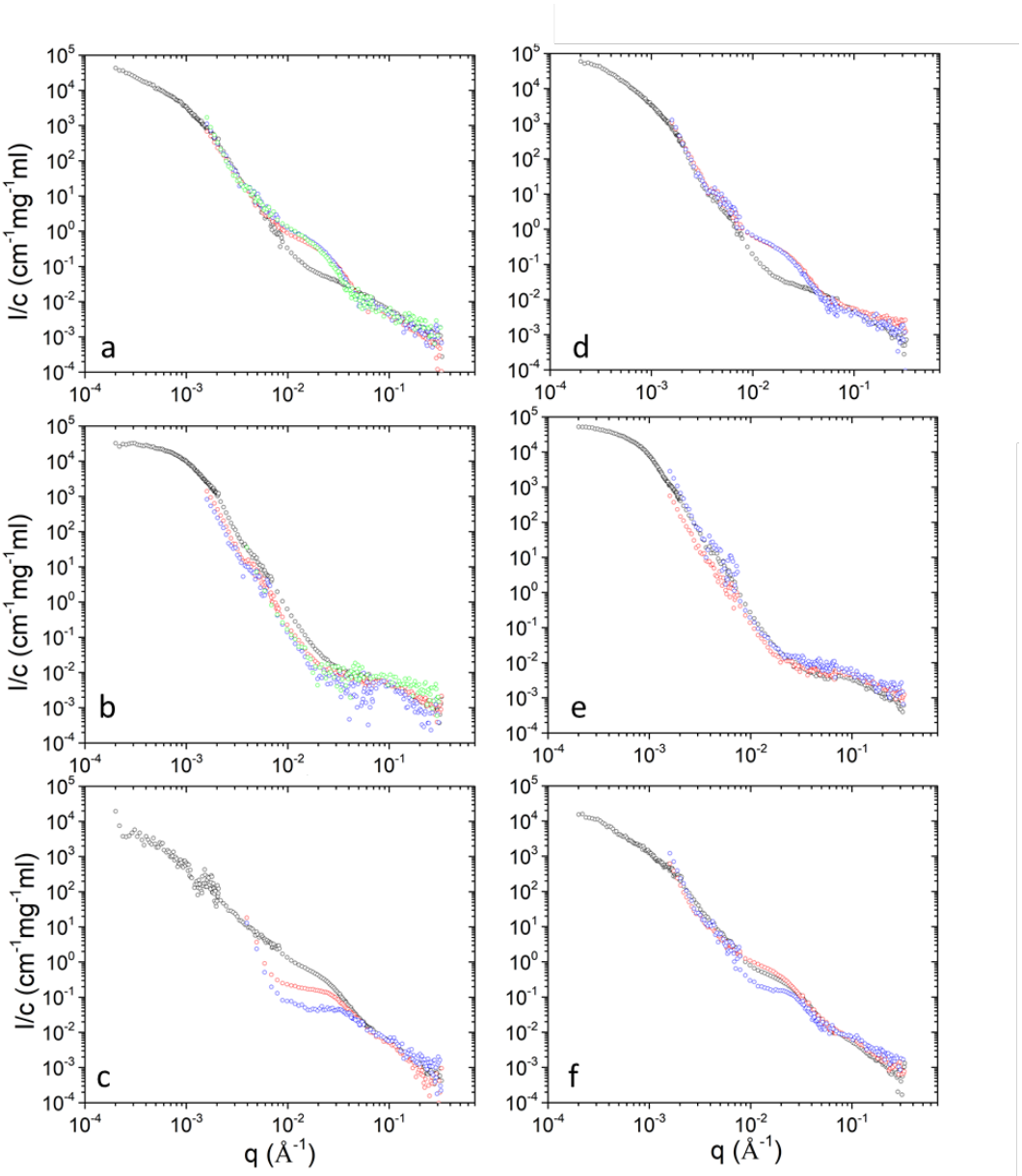

Figure 5. Concentration-normalized VS/SANS profiles at 45 °C from protocol A (a-c) and B (d-f) at pH 3 (a, d), pH7 (b, e) and pH 10 (c, f) at 0.5 (green), 1 (blue), 2 (red) and 4 (black) $mgml^{-1}$.

Concentration dependence of the self-assembled structures and their temperature response at lower concentrations was tested by diluting the 4 $mgml^{-1}$ samples at room temperature (Figure 5). In order to compare profiles from different concentrations the representation $I(q)/c$ is

chosen so that any trivial concentration effects are cancelled out. The shape of the VS/SANS profile for protocol A remains fairly unaltered only in the case of pH 7 (Figure 5b and e). There is a shift of the VS/SANS data to the left at intermediate q. This shows that there is a decrease of the contribution of the aggregates at this range. However, it cannot be deduced whether this is caused by an increase in the size of the aggregates or their mass. Data at low q is missing because of weak scattered intensity that did not allow collection of data on KWS-3 within reasonable time. Weak scattering also restricted data collection only down to 1 $mgml^{-1}$. At 0.5 $mgml^{-1}$ signal was too weak even at intermediate q (collected on KWS-2) and therefore analysis was not performed at this concentration. At 1 and 2 $mgml^{-1}$ at pH 10 a strong upturn at the lowest probed q seems to appear (Figure 5c and f). It is not certain that this is reliable as the data at lower q are missing. This could be a sign of formation of objects with smooth interface, but it will not be discussed further.

At pH 3 (Figure 5a and d) the appearance of small-size aggregates in the range $1 \cdot 10^{-2}$ $Å^{-1}$ to $7 \cdot 10^{-2}$ $Å^{-1}$ is observed in the diluted solutions. This reveals that in this complex dual-responsive system internal rearrangements are triggered by concentration alterations. Remarkably, a "reverse" effect is found at pH 10 (Figure 5c and f). The relative contribution from small-size aggregates gradually drops as concentration decreases. The discussion will focus on the evolution of the small-size aggregates at different concentrations (Table 5) as at higher q (small objects) there is no significant concentration dependence.

Table 5. VS/SANS-extracted parameters for small-size aggregates from PDMAEMA-b-PHPMA block copolymer solutions from different protocols at pH 3 and 10.

pH 3	
Parameter	G_3 (cm^{-1})

	protocol A				protocol B			
c (mgml^{-1})\ Temp. (°C)	25	35	45	55	25	35	45	55
1.0	1.24	1.40	1.50	1.58	1.00	1.10	1.17	1.18
2.0	1.53	1.64	1.75	1.87	0.823	1.61	1.63	0.951
Parameter	$R_{g,3}\ (nm)$							
	protocol A				protocol B			
c (mgml^{-1})\ Temp. (°C)	25	35	45	55	25	35	45	55
1.0	12.1	11.1	10.7	10.5	13.8	13.2	13.1	12.4
2.0	10.7	9.46	9.22	9.03	12.2	12.3	11.5	11.1

pH 10								
Parameter	$G_3\ (cm^{-1})$							
	protocol A				protocol B			
c (mgml^{-1})\ Temp. (°C)	25	35	45	55	25	35	45	55
1.0	-	-	-	0.0668	-	-	0.552	0.787
2.0	-	0.208	0.384	0.577	0.578	1.31	2.05	2.87
Parameter	$R_{g,3}\ (nm)$							
	protocol A				protocol B			
c (mgml^{-1})\ Temp. (°C)	25	35	45	55	25	35	45	55
1.0	-	-	-	5.23	-	-	24.1	24.7
2.0	-	6.87	7.34	8.15	12.4	8.86	9.56	10.7

Small-size aggregates at pH 3 have a size $R_{g,3} \approx 12\ nm$ (Table 5). Their forward scattering is between 1 and 2 cm^{-1} and shows a weak increase with temperature. The formation of small-size aggregates may be stimulated by a possible partial disintegration and rarefication of the

initial aggregates. This may allow a rearrangement of PDMAEMA units and self-assembly at larger length-scales in comparison to the small-size inhomogeneities.

At pH 10 small-size aggregates with $R_{g,3} \approx 8\,nm$ which is similar to the ones' appearing at pH 10 for 4 mgml^{-1} (Table 4). G_3 is in the order of 1-2 cm^{-1} These small-size aggregates appeared above room temperature at 4 mgml^{-1} for both preparation protocols. The sizes are not much different at lower concentrations except in protocol B at 1 mgml^{-1} where $R_{g,3} \approx 25\,nm$ (Tables 4 and 5). At 1 mgml^{-1} small-size aggregates in protocol A appear only at 55 °C and in B only at 45 and 55 °C. It can be deduced that small-size aggregates at this pH share the same mechanism of formation at all concentrations. At 2 mgml^{-1} they appear above 25 °C in A and at all temperatures in B. It can be assumed that at higher concentration small-size aggregates are more stable and may appear at lower temperatures. Forward scattering increases with temperature for both preparation protocols as at 4 mgml^{-1} at pH 3.

As VS/SANS did not provide strong scattering signal using VS/SANS at low concentrations we performed SLS experiments to explore whether the large-scale morphology (clusters and aggregates) still exist at lower concentrations. The optimal polymer concentration for SLS was 0.2 mgml^{-1} because it provided adequate scattered intensity and the solutions remained transparent at all pH conditions and temperatures. The accessible q-range of SLS ($6.8 \cdot 10^{-4}$ Å^{-1} to $2.6 \cdot 10^{-3}$ Å^{-1}) is restricted to the intermediate and low-q region of VS/SANS (Figure S2). However, the SLS profiles show that structure still forms at this length scales even at low concentration (in the opposite case Guinier behavior would be observed). The shape of the

reduced Rayleigh ratios from SLS R/Kc (referred to as I_{SLS} in Figure S2) is comparable to the SANS intensities. Although they are not in complete agreement, it is obvious that semi-quantitative characteristics are reproduced. The transition from the cluster to aggregate hierarchical level in Figures S1a and d, the transition from Guinier to power law regime in Figures S2b and e and the power law behavior in Figure S2c and the transition from cluster to aggregate scattering in Figure S2f are to a good degree reproduced by SLS.

4. Conclusions

VS/SANS was used to investigate the response of PDMAEMA-*b*-PHPMA assemblies to pH and temperature in aqueous solutions by preparation with two different protocols i.e. a solvent-exchange solubilization protocol and a direct solubilization protocol. The VS/SANS data were fitted by a generic hierarchical model that was based on the superposition of unified exponential/power-law scattering functions. Bayesian analysis was applied in order to quantify the parameters' interdependencies and to estimate their uncertainties. The analysis showed the existence of aggregates consisting of a network of inhomogeneities and being able to form hierarchically structured clusters depending on pH. The temperature response of the different structural levels depended on pH and preparation protocol. This work demonstrates the use of VS/SANS for the elucidation of internal arrangements in doubly responsive block copolymer aggregates and it has direct implications in interactions with molecular drugs and biological macromolecules.

5. Acknowledgements

This work is based upon experiments performed at the KWS-2 and KWS-3 instruments operated by JCNS at the Heinz Maier-Leibnitz Zentrum (MLZ), Garching, Germany.

6. References

[1] J.-F. Gohy, Block Copolymer Micelles, in: V. Abetz (Ed.), Block Copolymers II, Springer Berlin Heidelberg, Berlin, Heidelberg, 2005, pp. 65-136.

[2] G. Gaucher, M.H. Dufresne, V.P. Sant, N. Kang, D. Maysinger, J.C. Leroux, Block copolymer micelles: preparation, characterization and application in drug delivery, J Control Release 109(1-3) (2005) 169-88.

[3] Y. Mai, A. Eisenberg, Self-assembly of block copolymers, Chem Soc Rev 41(18) (2012) 5969-85.

[4] A. Blanazs, S.P. Armes, A.J. Ryan, Self-Assembled Block Copolymer Aggregates: From Micelles to Vesicles and their Biological Applications, Macromol Rapid Commun 30(4-5) (2009) 267-77.

[5] A.E. Smith, X. Xu, C.L. McCormick, Stimuli-responsive amphiphilic (co)polymers via RAFT polymerization, Progress in Polymer Science 35(1-2) (2010) 45-93.

[6] A.O. Moughton, T. Sagawa, L. Yin, T.P. Lodge, M.A. Hillmyer, Multicompartment Micelles by Aqueous Self-Assembly of μ-A(BC)n Miktobrush Terpolymers, ACS Omega 1(5) (2016) 1027-1033.

[7] K.K. Upadhyay, H.G. Agrawal, C. Upadhyay, C. Schatz, J.F. Le Meins, A. Misra, S. Lecommandoux, Role of block copolymer nanoconstructs in cancer therapy, Crit Rev Ther Drug Carrier Syst 26(2) (2009) 157-205.

[8] M.M. Lubtow, H. Marciniak, A. Schmiedel, M. Roos, C. Lambert, R. Luxenhofer, Ultra-High to Ultra-Low Drug-Loaded Micelles: Probing Host-Guest Interactions by Fluorescence Spectroscopy, Chemistry 25(54) (2019) 12601-12610.

[9] M. Hruby, P. Štěpánek, J. Pánek, C.M. Papadakis, Crosstalk between responsivities to various stimuli in multiresponsive polymers: change in polymer chain and external

environment polarity as the key factor, Colloid and Polymer Science 297(11-12) (2019) 1383-1401.

[10] A.E. Smith, X. Xu, S.E. Kirkland-York, D.A. Savin, C.L. McCormick, “Schizophrenic” Self-Assembly of Block Copolymers SynthesizedviaAqueous RAFT Polymerization: From Micelles to Vesicles in a series on Water-Soluble Polymers, Macromolecules 43(3) (2010) 1210-1217.

[11] N.S. Vishnevetskaya, V. Hildebrand, M.A. Dyakonova, B.-J. Niebuur, K. Kyriakos, K.N. Raftopoulos, Z. Di, P. Müller-Buschbaum, A. Laschewsky, C.M. Papadakis, Dual Orthogonal Switching of the “Schizophrenic” Self-Assembly of Diblock Copolymers, Macromolecules 51(7) (2018) 2604-2614.

[12] V. Hildebrand, M. Heydenreich, A. Laschewsky, H.M. Möller, P. Müller-Buschbaum, C.M. Papadakis, D. Schanzenbach, E. Wischerhoff, “Schizophrenic” self-assembly of dual thermoresponsive block copolymers bearing a zwitterionic and a non-ionic hydrophilic block, Polymer 122 (2017) 347-357.

[13] V. Chrysostomou, S. Pispas, Stimuli-responsive amphiphilic PDMAEMA-b-PLMA copolymers and their cationic and zwitterionic analogs, Journal of Polymer Science Part A: Polymer Chemistry 56(6) (2018) 598-610.

[14] J. Niskanen, C. Wu, M. Ostrowski, G.G. Fuller, S. Hietala, H. Tenhu, Thermoresponsiveness of PDMAEMA. Electrostatic and Stereochemical Effects, Macromolecules 46(6) (2013) 2331-2340.

[15] A. Skandalis, S. Pispas, PDMAEMA-b-PLMA-b-POEGMA triblock terpolymers via RAFT polymerization and their self-assembly in aqueous solutions, Polymer Chemistry 8(31) (2017) 4538-4547.

[16] S. Agarwal, Y. Zhang, S. Maji, A. Greiner, PDMAEMA based gene delivery materials, Materials Today 15(9) (2012) 388-393.

[17] A.P. Majewski, U. Stahlschmidt, V. Jerome, R. Freitag, A.H. Muller, H. Schmalz, PDMAEMA-grafted core-shell-corona particles for nonviral gene delivery and magnetic cell separation, Biomacromolecules 14(9) (2013) 3081-90.

[18] O. Samsonova, C. Pfeiffer, M. Hellmund, O.M. Merkel, T. Kissel, Low Molecular Weight pDMAEMA-block-pHEMA Block-Copolymers Synthesized via RAFT-Polymerization: Potential Non-Viral Gene Delivery Agents?, Polymers 3(2) (2011) 693-718.

[19] C. Zhu, M. Zheng, F. Meng, F.M. Mickler, N. Ruthardt, X. Zhu, Z. Zhong, Reversibly shielded DNA polyplexes based on bioreducible PDMAEMA-SS-PEG-SS-PDMAEMA triblock copolymers mediate markedly enhanced nonviral gene transfection, Biomacromolecules 13(3) (2012) 769-78.

[20] C.J. Mable, K.L. Thompson, M.J. Derry, O.O. Mykhaylyk, B.P. Binks, S.P. Armes, ABC Triblock Copolymer Worms: Synthesis, Characterization, and Evaluation as Pickering Emulsifiers for Millimeter-Sized Droplets, Macromolecules 49(20) (2016) 7897-7907.

[21] N.J. Warren, O.O. Mykhaylyk, D. Mahmood, A.J. Ryan, S.P. Armes, RAFT aqueous dispersion polymerization yields poly(ethylene glycol)-based diblock copolymer nano-objects with predictable single phase morphologies, J Am Chem Soc 136(3) (2014) 1023-33.

[22] R. Verber, A. Blanazs, S.P. Armes, Rheological studies of thermo-responsive diblock copolymer worm gels, Soft Matter 8(38) (2012).

[23] J.R. Lovett, L.P. Ratcliffe, N.J. Warren, S.P. Armes, M.J. Smallridge, R.B. Cracknell, B.R. Saunders, A Robust Cross-Linking Strategy for Block Copolymer Worms Prepared via Polymerization-Induced Self-Assembly, Macromolecules 49(8) (2016) 2928-2941.

[24] N.S. Vishnevetskaya, V. Hildebrand, B.-J. Niebuur, I. Grillo, S.K. Filippov, A. Laschewsky, P. Müller-Buschbaum, C.M. Papadakis, Aggregation Behavior of Doubly Thermoresponsive Polysulfobetaine-b-poly(N-isopropylacrylamide) Diblock Copolymers, Macromolecules 49(17) (2016) 6655-6668.

[25] N.S. Vishnevetskaya, V. Hildebrand, B.-J. Niebuur, I. Grillo, S.K. Filippov, A. Laschewsky, P. Müller-Buschbaum, C.M. Papadakis, “Schizophrenic” Micelles from Doubly Thermoresponsive Polysulfobetaine-b-poly(N-isopropylmethacrylamide) Diblock Copolymers, Macromolecules 50(10) (2017) 3985-3999.

[26] Y.J. Shih, Y. Chang, A. Deratani, D. Quemener, "Schizophrenic" hemocompatible copolymers via switchable thermoresponsive transition of nonionic/zwitterionic block self-assembly in human blood, Biomacromolecules 13(9) (2012) 2849-58.

[27] T. Sentoukas, S. Pispas, Poly(dimethylaminoethyl methacrylate)-b-poly(hydroxypropyl methacrylate) copolymers: Synthesis and pH/thermo-responsive behavior in aqueous solutions, Journal of Polymer Science Part A: Polymer Chemistry 56(17) (2018) 1962-1977.

[28] T. Sentoukas, S. Pispas, Poly(2-(dimethylamino)ethyl methacrylate)-b-poly(hydroxypropyl methacrylate) copolymers/bovine serum albumin complexes in aqueous solutions, Journal of Polymer Science 58(9) (2020) 1241-1252.

[29] T. Sentoukas, S. Pispas, Poly(2-[dimethylamino]ethyl methacrylate)-b-poly(hydroxypropyl methacrylate)/DNA polyplexes in aqueous solutions, Journal of Polymer Science 58(17) (2020) 2335-2346.

[30] S.K. Filippov, A. Bogomolova, L. Kaberov, N. Velychkivska, L. Starovoytova, Z. Cernochova, S.E. Rogers, W.M. Lau, V.V. Khutoryanskiy, M.T. Cook, Internal Nanoparticle Structure of Temperature-Responsive Self-Assembled PNIPAM-b-PEG-b-PNIPAM Triblock Copolymers in Aqueous Solutions: NMR, SANS, and Light Scattering Studies, Langmuir 32(21) (2016) 5314-5323.

[31] M.T. Cook, S.K. Filippov, V.V. Khutoryanskiy, Synthesis and solution properties of a temperature-responsive PNIPAM–b-PDMS–b-PNIPAM triblock copolymer, Colloid and Polymer Science 295(8) (2017) 1351-1358.

[32] S. Jaksch, A. Schulz, K. Kyriakos, J. Zhang, I. Grillo, V. Pipich, R. Jordan, C.M. Papadakis, The collapse and aggregation of thermoresponsive poly(2-oxazoline) gradient copolymers: a time-resolved SANS study, Colloid and Polymer Science 292(10) (2014) 2413-2425.

[33] J.-J. Kang, K. Shehu, C. Sachse, F.A. Jung, C.-H. Ko, L.C. Barnsley, R. Jordan, C.M. Papadakis, A molecular brush with thermoresponsive poly(2-ethyl-2-oxazoline) side chains: a structural investigation, Colloid and Polymer Science (2020).

[34] L. Bondaz, P. Fontaine, F. Muller, N. Pantoustier, P. Perrin, I. Morfin, M. Goldmann, F. Cousin, Controlled Synthesis of Gold Nanoparticles in Copolymers Nanomolds by X-ray Radiolysis, Langmuir 36(22) (2020) 6132-6144.

[35] A. Papagiannopoulos, E. Vlassi, A. Radulescu, Reorganizations inside thermally stabilized protein/polysaccharide nanocarriers investigated by small angle neutron scattering, Carbohydr Polym 218 (2019) 218-225.

[36] A. Papagiannopoulos, A. Meristoudi, S. Pispas, U. Keiderling, Thermoresponsive behavior of micellar aggregates from end-functionalized PnBA-b-PNIPAM-COOH block copolymers and their complexes with lysozyme, Soft Matter 12(31) (2016) 6547-56.

[37] S. Jaksch, A. Schulz, Z. Di, R. Luxenhofer, R. Jordan, C.M. Papadakis, Amphiphilic Triblock Copolymers from Poly(2-oxazoline) with Different Hydrophobic Blocks: Changes of the Micellar Structures upon Addition of a Strongly Hydrophobic Cancer Drug, Macromolecular Chemistry and Physics 217(13) (2016) 1448-1456.

[38] B. Sochor, Ö. Düdükcü, M.M. Lübtow, B. Schummer, S. Jaksch, R. Luxenhofer, Probing the Complex Loading-Dependent Structural Changes in Ultrahigh Drug-Loaded Polymer Micelles by Small-Angle Neutron Scattering, Langmuir 36(13) (2020) 3494-3503.

[39] M. Hrubý, S.K. Filippov, P. Štěpánek, Smart polymers in drug delivery systems on crossroads: Which way deserves following?, European Polymer Journal 65 (2015) 82-97.

[40] A. Papagiannopoulos, A. Meristoudi, S. Pispas, U. Keiderling, Thermal response of self-organization in an amphiphilic triblock polyelectrolyte and the influence of the globular protein lysozyme, European Polymer Journal 99 (2018) 49-57.

[41] K.A. Rubinson, Practical corrections for p(H,D) measurements in mixed H2O/D2O biological buffers, Analytical Methods 9(18) (2017) 2744-2750.

[42] J.G. Barker, J.S. Pedersen, Instrumental Smearing Effects in Radially Symmetric Small-Angle Neutron Scattering by Numerical and Analytical Methods, Journal of Applied Crystallography 28(2) (1995) 105-114.

[43] A. Radulescu, N.K. Szekely, S. Polachowski, M. Leyendecker, M. Amann, J. Buitenhuis, M. Drochner, R. Engels, R. Hanslik, G. Kemmerling, P. Lindner, A. Papagiannopoulos, V. Pipich, L. Willner, H. Frielinghaus, D. Richter, Tuning the instrument resolution using chopper and time of flight at the small-angle neutron scattering diffractometer KWS-2, J Appl Crystallogr 48(Pt 6) (2015) 1849-1859.

[44] T. Vad, W.F.C. Sager, J. Zhang, J. Buitenhuis, A. Radulescu, Experimental determination of resolution function parameters from small-angle neutron scattering data of a colloidal SiO2dispersion, Journal of Applied Crystallography 43(4) (2010) 686-692.

[45] D. Vanderbilt, S.G. Louie, A Monte carlo simulated annealing approach to optimization over continuous variables, Journal of Computational Physics 56(2) (1984) 259-271.

[46] J. Goodman, J. Weare, Ensemble samplers with affine invariance, Commun. Appl. Math. Comput. Sci. 5(1) (2010) 65-80.

[47] S.W. Winslow, W. Shcherbakov-Wu, Y. Liu, W.A. Tisdale, J.W. Swan, Characterization of colloidal nanocrystal surface structure using small angle neutron scattering and efficient Bayesian parameter estimation, The Journal of Chemical Physics 150(24) (2019) 244702.

[48] W. Adler, Cornerplot, 2018. https://nl.mathworks.com/matlabcentral/fileexchange/49567-cornerplot.

[49] B. Chu, Laser Light Scattering Basic Principles and Practice, Academic Press1991.

[50] E.M. Anitas, Small-Angle Scattering from Fractals: Differentiating between Various Types of Structures, Symmetry 12(1) (2020).

[51] A. Papagiannopoulos, Investigations of Complex Polymer-based Nanoassemblies with Small Angle Neutron Scattering, in: A. Reimer (Ed.), Nova Science Publishers2017.

[52] J. Madsen, S.P. Armes, K. Bertal, S. MacNeil, A.L. Lewis, Preparation and aqueous solution properties of thermoresponsive biocompatible AB diblock copolymers, Biomacromolecules 10(7) (2009) 1875-87.

[53] D.C. Dong, M.A. Winnik, THE Py SCALE OF SOLVENT POLARITIES. SOLVENT EFFECTS ON THE VIBRONIC FINE STRUCTURE OF PYRENE FLUORESCENCE and EMPIRICAL CORRELATIONS WITH ET and Y VALUES, Photochemistry and Photobiology 35(1) (1982) 17-21.

[54] M. Johnsson, P. Hansson, K. Edwards, Spherical Micelles and Other Self-Assembled Structures in Dilute Aqueous Mixtures of Poly(Ethylene Glycol) Lipids, The Journal of Physical Chemistry B 105(35) (2001) 8420-8430.

[55] T. Wu, J. Oake, Z. Liu, C. Bohne, N.R. Branda, Probing the Microenvironments in a Polymer-Wrapped Core–Shell Nanoassembly Using Pyrene Chromophores, ACS Omega 3(7) (2018) 7673-7680.

[56] F.A. Plamper, M. Ruppel, A. Schmalz, O. Borisov, M. Ballauff, A.H.E. Müller, Tuning the Thermoresponsive Properties of Weak Polyelectrolytes: Aqueous Solutions of Star-Shaped and Linear Poly(N,N-dimethylaminoethyl Methacrylate), Macromolecules 40(23) (2007) 8361-8366.

[57] J. Madsen, S.P. Armes, A.L. Lewis, Preparation and Aqueous Solution Properties of New Thermoresponsive Biocompatible ABA Triblock Copolymer Gelators, Macromolecules 39(22) (2006) 7455-7457.

[58] A. Blanazs, R. Verber, O.O. Mykhaylyk, A.J. Ryan, J.Z. Heath, C.W. Douglas, S.P. Armes, Sterilizable gels from thermoresponsive block copolymer worms, J Am Chem Soc 134(23) (2012) 9741-8.

[59] P. Schmidt, Small-angle scattering studies of disordered, porous and fractal systems, Journal of Applied Crystallography 24(5) (1991) 414-435.

[60] J. Oberdisse, W. Pyckhout-Hintzen, E. Straube, Structure Determination of Polymer Nanocomposites by Small Angle Scattering, in: G.E.Z. S. Thomas, S.V. Valsaraj (Eds.), Recent Advances in Polymer Nanocomposites, Brill2009, p. 397.

[61] G. Beaucage, D.W. Schaefer, Structural studies of complex systems using small-angle scattering: a unified Guinier/power-law approach, Journal of Non-Crystalline Solids 172-174 (1994) 797-805.

[62] A. Papagiannopoulos, M. Karayianni, G. Mountrichas, S. Pispas, A. Radulescu, Micellar and fractal aggregates formed by two triblock terpolymers with different arrangements of one charged, one neutral hydrophilic and one hydrophobic block, Polymer 63 (2015) 134-143.

[63] F. Horkay, G.B. McKenna, P. Deschamps, E. Geissler, Neutron Scattering Properties of Randomly Cross-Linked Polyisoprene Gels, Macromolecules 33(14) (2000) 5215-5220.

[64] S. Panyukov, Y. Rabin, Polymer Gels: Frozen Inhomogeneities and Density Fluctuations, Macromolecules 29(24) (1996) 7960-7975.

[65] M. Shibayama, Small-angle neutron scattering on polymer gels: phase behavior, inhomogeneities and deformation mechanisms, Polymer Journal 43(1) (2011) 18-34.

[66] M. Shibayama, H. Kurokawa, S. Nomura, M. Muthukumar, R.S. Stein, S. Roy, Small-angle neutron scattering from poly(vinyl alcohol)-borate gels, Polymer 33(14) (1992) 2883-2890.

[67] D.W. Schaefer, T. Rieker, M. Agamalian, J.S. Lin, D. Fischer, S. Sukumaran, C. Chen, G. Beaucage, C. Herd, J. Ivie, Multilevel structure of reinforcing silica and carbon, Journal of Applied Crystallography 33(3 Part 1) (2000) 587-591.

[68] M. Wagner, C. Pietsch, A. Kerth, A. Traeger, U.S. Schubert, Physicochemical characterization of the thermo-induced self-assembly of thermo-responsive PDMAEMA-b-PDEGMA copolymers, Journal of Polymer Science Part A: Polymer Chemistry 53(7) (2015) 924-935.

[69] H. Mao, C. Li, Y. Zhang, S. Furyk, P.S. Cremer, D.E. Bergbreiter, High-Throughput Studies of the Effects of Polymer Structure and Solution Components on the Phase Separation of Thermoresponsive Polymers, Macromolecules 37(3) (2004) 1031-1036.

[70] P. Kujawa, F.M. Winnik, Volumetric Studies of Aqueous Polymer Solutions Using Pressure Perturbation Calorimetry: A New Look at the Temperature-Induced Phase Transition of Poly(N-isopropylacrylamide) in Water and D2O, Macromolecules 34(12) (2001) 4130-4135.

[71] A.E. Felber, M.H. Dufresne, J.C. Leroux, pH-sensitive vesicles, polymeric micelles, and nanospheres prepared with polycarboxylates, Adv Drug Deliv Rev 64(11) (2012) 979-92.